A Quantum Mechanical Investigation of Possible Mechanisms for the Nucleotidyl Transfer Reaction Catalyzed by DNA Polymerase β

Mihaela D. Bojin and Tamar Schlick*

Department of Chemistry and the Courant Institute of Mathematical Sciences, New York University, 251 Mercer Street, New York, New York 10012

Received: March 6, 2007; In Final Form: July 9, 2007

Several quantum mechanical (QM) and hybrid quantum/molecular mechanical (QM/MM) studies have been employed recently to analyze the nucleotidyl transfer reaction in DNA polymerase β (pol β). Our examination reveals strong dependence of the reported mechanism on the initial molecular model. Thus, we explore here several model systems by QM methods to investigate pol β's possible pathway variations. Although our most favorable pathway involves a direct proton transfer from O3′(primer) to $O2_\alpha(P_\alpha)$, we also discuss other initial proton-transfer steps—to an adjacent water, to triphosphate, or to aspartic units—and the stabilizing effect of crystallographic water molecules in the active site. Our favored reaction route has an energetically undemanding initial step of less than 1.0 kcal/mol (at the B3LYP/6-31G(d,p) level), and involves a slight rearrangement in the geometry of the active site. This is followed by two major steps: (1) direct proton transfer from O3′(primer) to $O2_\alpha(P_\alpha)$ leading to the formation of a pentavalent, trigonal bipyramidal P_α center, via an associative mechanism, at a cost of about 28 kcal/mol, and (2) breakage of the triphosphate unit (exothermic process, ∼22 kcal/mol) that results in the full transfer of the nucleotide to the DNA and the formation of pyrophosphate. These energy values are expected to be lower in the physical system when full protein effects are incorporated. We also discuss variations from this dominant pathway, and their impact on the overall repair process. Our calculated barrier for the chemical reaction clearly indicates that chemistry is rate-limiting overall for correct nucleotide insertion in pol β, in accord with other studies. Protonation studies on relevant intermediates suggest that, although protonation at a single aspartic residue may occur, the addition of a second proton to the system significantly disturbs the active site. We conclude that the active site rearrangement step necessary to attain a reaction-competent geometry is essential and closely related to the "pre-chemistry" avenue described recently as a key step in the overall kinetic cycle of DNA polymerases. Thus, our work emphasizes the many possible ways for DNA polymerase β's chemical reaction to occur, determined by the active site environment and initial models.

Introduction

DNA polymerases play an essential role in maintaining the integrity of the human genome by repairing damaged DNA.[1−3] Such repair is realized following a general pathway, which involves two ions—often magnesiums—one termed "catalytic" and the other "nucleotide-binding".[4−8] Mg^{2+}_{cat} is recognized as being critical during catalysis, whereas Mg^{2+}_{nuc} provides the architectural framework to support the triphosphate ligand, which carries the incoming nucleotide.[9]

Mammalian DNA polymerase β (pol β), in the X-family, has been thoroughly studied both experimentally and theoretically, due to its biological importance and relatively modest size (39 kDa). Pol β contains 335 protein residues, assembled in two major domains: a 31 kDa C-terminal region, with nucleotidyl transferase activity, composed of three different hand-like components—"thumb", "palm", and "fingers" subdomains—and an 8 kDa N-terminal region that exhibits deoxyribose phosphate lyase activity.[10,11]

Several exquisite crystal structures, along with extensive kinetic data and computational modeling, have provided the basis for understanding the mechanism of pol β and created a bridge between pol β's structure/flexibility and function.

Two ternary structures were reported in 1994[11c] for a rat DNA polymerase β, which contained the DNA, template-primer, and ddCTP, determined at 2.9 and 3.6 Å resolution. A later refined structural study on a human pol β complex, PDB entry *1bpy* (2.2 Å resolution),[10−11] provided the first accurate look into the closed ternary system (polymerase β, DNA, and incoming nucleotide). The complex lacked the catalytic Mg^{2+}, but captured one sodium ion. It contained 2′,3′-dideoxycytidine-5′-triphosphate (ddCTP), as substitute for the incoming 2′-deoxyribonucleoside-5′-triphosphate (dNTP), but did not yet resolve all critical water molecules in the active site, due to the limited resolution available at the time. Further refinement of this structure, determined at 1.65 Å resolution (PDB entry *2fmp*), led to a complex that resolved the position of the water molecules in the active site, and thus the coordination around the catalytic ion.[12] Additional structures with mismatched DNA base pairs for the apoenzyme[11c] or lesion-containing[11d] bound DNA were later reported and shed light on the insertion mechanism of pol β and its fidelity; their active sites also lacked the OH groups on the primer and incoming nucleotidic base pairs.[13−15] The latest crystal complex[12] (2.0 Å resolution) is remarkable in that it has both Mg^{2+} in the active site along with the formerly missing OH groups. However, in place of a naturally occurring dNTP, this new structure contains 2′-deoxy-

* Address correspondence to this author. E-mail: schlick@nyu.edu.

10.1021/jp071838c CCC: $37.00
Published on Web 09/01/2007

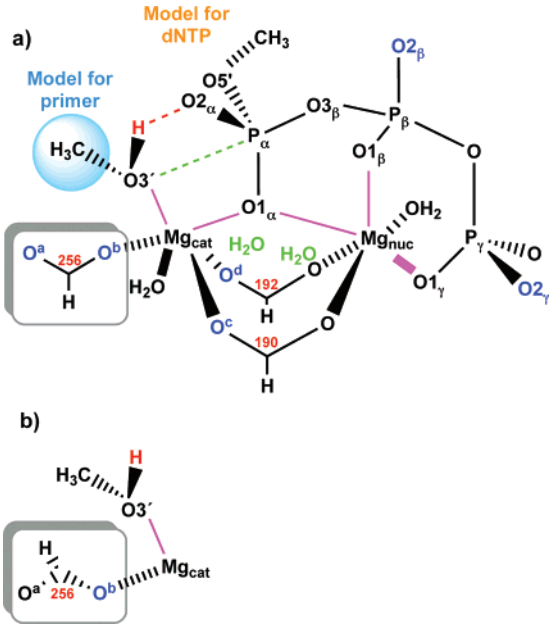

Figure 1. Active site of pol β with relevant notation for main atoms. Highlighted in blue are the seven protonation positions investigated in this work, six in part a and one in part b. The dihedral angle (O3′−Mg_{cat}−O^b−C^{256}) is 0° in part a and 90° in part b. Unbound crystallographic water molecules are in green in part a.

uridine-5′-[(α,β)-imido]triphosphate (dUMPNPP), which cannot be hydrolyzed.

Several modeling works anchored in these crystal structures have addressed the repair mechanism of pol β, using various computational methods. Molecular dynamics (MD) simulations[16,18] revealed that an induced-fit mechanism is responsible for the rearrangement of the C-terminal subdomain upon binding the correct substrate and delineated specific conformational changes that occur in the closing pathway of pol β. Modeling also demonstrated how an incorrect nucleotide inserted in the DNA introduces geometric deformations in the active site that hamper conformational closing before the chemical reaction.[17,20] Transition path sampling (TPS) simulations[19] further revealed the major domain motions, associated transition states, and energies of polymerase β's closing pathway. They also showed how the pathway for a correct G:C system differs from that for an incorrect G:A base pair and that the stability of the closed state relative to the open state determines the evolution of substrate to product in the overall pathway.[20a] A recent review[20b] detailed the emerging concept of "pre-chemistry", which occurs after conformational changes, but prior to the chemical reaction, and may be key to interpreting fidelity discrimination across polymerases through kinetic checkpoints.

Aside from large domain motions and subtle local conformational rearrangements in pol β, additional transformations in the active site occur toward and during catalysis. Investigating this chemical step, which involves bond breaking/forming events, requires computational techniques beyond classical mechanics to capture electronic changes, namely quantum mechanical (QM), or mixed quantum mechanics and molecular mechanics (QM/MM) methods.

Several groups have reported various aspects of the chemical step in nucleotide incorporation for pol β by such methods.[20−23] Each study differed in its initial model, which strongly influenced QM and QM/MM calculations. In addition to defining the molecular system, the initial steps of the reaction have been set up differently across these reported studies.

A sketch of the active site of pol β is given in Figure 1. As accepted in standard terminology, O3′ refers to the attacking nucleophile of the primer terminus oxygen atom and O5′ to the oxygen atom of the dNTP that connects the deoxyribose ring with the triphosphate moiety. $O1_\alpha$, $O1_\beta$, and $O1_\gamma$ are oxygens on P_α, P_β, and P_γ coordinated to the magnesium ions; $O2_\alpha$, $O2_\beta$, and $O2_\gamma$ designate terminal oxygens on P_α, P_β, and P_γ; and $O3_\beta$ bridges P_α to P_β.

Ideally, the active site model should possess two magnesium ions, each surrounded by six ligands, in an octahedral setting. The coordination sphere of the catalytic Mg^{2+}_{cat} has six oxygen atoms: (1) O3′ primer, (2) $O1_\alpha$ (oxygen on the P_α of triphosphate), (3) one water molecule ($H_2O(1)$), and (4) an oxygen of D256 residue (D = aspartic residue, or Asp), (5) of D190, and (6) of D192. The nucleotide-binding Mg^{2+}_{nuc} is linked to oxygen atoms of residues: (1) D190, (2) D192, (3) $O1_\alpha(P_\alpha)$, (4) $O1_\beta$-(P_β), (5) $O1_\gamma(P_\gamma)$, and (6) a water molecule.

As mentioned above, not all residues are present in the experimental structures published to date, and thus some creativity is required for constructing accurate initial model complexes to elucidate the chemical step.

In an early QM investigation, Abashkin and collaborators[21] used a starting model for the active site that had an HO^-, instead of D256 coordinated to the catalytic Mg^{2+}, no crystallographic water molecules, and only one water molecule coordinated to the nucleotidic magnesium ions. D192 was protonated. This model departed from the experimental active site, as it had only five ligands around the catalytic Mg^2 ion. The authors proposed that the reaction followed an associative pathway initiated by a transfer of the H^+ from O3′ to $O2_\alpha(P_\alpha)$, and involved the formation of a five-coordinated P_α transition state along with several other intermediates on the potential surface.

Rittenhouse et al.[22] used MD and QM techniques to investigate the role of the missing O3′H groups from primer and nucleotide. Their models included all relevant ligands and one noncovalently bound water molecule. They also suggested an associative pathway, but did not trace the main intermediates along the reaction pathway. Several protonation sites were analyzed, and the presence of an additional H^+ in the active site, most likely on D256, could not be ruled out.

Lin et al.[23a] recently employed QM/MM to study the active site of a variant of pol β. This system had as incoming nucleotide 2′-deoxy-thymine-triphosphate (dTTP) opposite an A template (A:T base pair), instead of dCTP opposite a G template, and included the O3′H groups on the primer and nucleotidic ribose rings. The QM region of this complex had an unusually coordinated O3′H to the Mg^{2+}_{cat} ion, in which the hydrogen pointed toward D256, and not in the direction of $O2_\alpha(P_\alpha)$, as previously considered.[21,22] Apart from this detail concerning the directionality of this hydrogen bond, the rest of the structure is nearly identical with the Rittenhouse et al.[22] model. The authors suggested an initial step involving a direct shift of the proton from O3′ to D256 and located, via a series of constrained optimizations, a transition state with a pentavalent P_α center, 21.5 kcal/mol higher than their initial complex, at the B3LYP/6-31G(d) level, for the QM region of the QM/MM computation.

Radhakrishnan and Schlick[23b] developed a combined QM/MM and MD approach and analyzed in detail yet another pathway, for both matched and mismatched pol β/DNA systems (i.e., G:C and G:A nascent base pairs). The active site derived from the *1bpy* (lower resolution structure of pol β) included two unbound waters whose positions were determined from MD simulations. The initial step, deprotonation of O3′, occurs via mediation of two crystallographic waters; namely, a Grotthuss

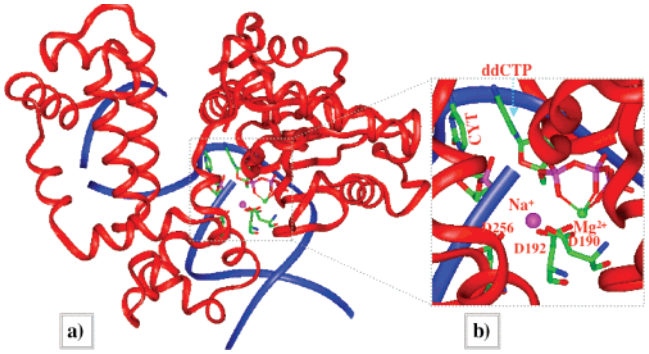

Figure 2. (a) Ribbon structure of polymerase β (PDB entry: *2fmp*). The DNA chain is blue and the protein red. In the gray dotted box is the active site region, and in part b a zoom into in it, with labels for relevant residues and ions. Water molecules are not shown for clarity.

type mechanism was followed in which the proton hopped to D192, D190, and finally to $O2_\gamma(P_\gamma)$. An intermediate with a pentavalent P_α was located, about 18.0 kcal/mol higher in energy than the initial complex (B3LYP/6-311G level, for the QM region), as well as products resulting from the dissociation of the triphosphate. On the basis of a prior path sampling study[20a] and QM/MM minimizations on the initial geometry of pol β's active site, Radhakrishnan and Schlick also suggested that two of the crystallographic water molecules could be involved in the proton abstraction from O3′ to D256. This proposed mechanism concurs with computations described by Warshel et al.[24−26]

Warshel et al.[24−26] used the empirical valence bond (EVB) method to study catalysis in Polymerase I and T7 DNA polymerases. Although the active sites of these polymerases are similar to that of pol β, details are different: T7 has two aspartates (three for pol β) and no water molecules coordinated to Mg^{2+} ions, whereas Pol I has only one aspartate bridging the magnesium ions and two other aspartates acting as terminal ligands on each of the two Mg^{2+} ions. Warshel and co-workers discussed in detail variations for initiating the chemical step of T7, H^+ transfer from O3′ to (1) the crystallographic waters, (2) $O2_\alpha(P_\alpha)$, or (3) an adjacent aspartate. They considered the last scenario most favorable, and estimated an activation barrier of about 12 kcal/mol; the transition state had a pentavalent phosphorus (P_α) atom.[25]

Clearly, the choice of initial structure significantly affects the reaction mechanism. A water molecule in the immediate vicinity of O3′H, with potential to form a direct hydrogen bond, may critically influence the preferred pathway. The exact positions of these water molecules are difficult to determine due to the dynamic nature of water in the active site. Thus, various possibilities remain viable.

Our QM study considers several model systems based on the high-resolution (1.65 Å, *2fmp*) pol β complex,[12] modified to best represent its active site by including all its key structural elements. For that reason, we add the missing O3′H residues, replace the Na^+ from the catalytic position with a Mg^{2+} ion, and retain two of the crystallographic, noncovalently bound water molecules (Figure 2). These changes lead to hexacoordinated magnesium ions.

We find a favored associative mechanism and specific intermediates along the pathway in pol β's cycle. This route requires an initial reorganization step, direct H^+ migration from O3′ to $O2_\alpha(P_\alpha)$, which leads to an intermediate with a pentavalent P_α (related to a possible transition state), followed by the breaking of the triphosphate moiety.

To reach these conclusions, we also examined several different pathways described in the works mentioned above, namely for the initial step of H^+ migration from O3′ to D256, D190, and D192, and to $H_2O(1)$ coordinated to $Mg^{2+}{}_{cat}$. We find that all are energetically less favorable than direct transfer to $O2_\alpha(P_\alpha)$, and present the main reaction coordinate that links relevant intermediates for this most favorable pathway. We also analyzed systematically seven possible protonation positions in our complexes by investigating key protonated intermediates and the associated relative energies. Finally, we examine the possibility of adding two protons to the active site. The main text describes the preferred pathway, while the protonation studies are collected in the Appendix. Though QM studies neglect the full protein/DNA environment in favor of a representative model system, they allow us to evaluate in greater detail the likelihood of related or alternative mechanistic pathways.

Methods

QM Methods. All ab initio and density functional computations (DFT) were performed with the Gaussian program, versions 03 and 98.[34] We perform full optimizations on all structures (no constraints were imposed on any of these systems) in the gas phase, using two functionals, the hybrid Hartree−Fock (HF)−density functional theory (DFT), B3LYP, as well as HF, with two basis sets: 6-31G and 6-31G(d,p); the latter basis set includes polarization effects that become significant when noncovalent or weakly covalent interactions are present.[28,31] We include the crystallographic water molecules to account for specific solvent effects. Additionally, we re-optimize our main intermediates using the electron-correlated Møller−Plesset perturbation theory,[30] MP2, with the 6-31G basis set. The more expensive B3LYP and MP techniques yield similar structures to those obtained with the minimal but faster HF method. While modifying the functional did not produce significant variations in terms of relative energies, the increase in basis set led to higher energies, but consistent structural and energetic trends. These results are summarized in Table S1a of the Supporting Information.

Frequency analyses are performed on all stationary points, and the reported energies include zero-point energy corrections (ZPE) (unscaled). The relative energies (B3LYP/6-31G(d,p) level) on the constrained potential energy surfaces do not include ZPE corrections, as frequency analyses on these complexes are not physically meaningful.

The energies reported in the main text for the fully optimized structures **A**−**G** (our main intermediates) were obtained by using the B3LYP/6-31G(d,p) method (Gaussian 03), and include ZPE corrections (as they are local minima). We employed the lower accuracy, but faster, HF/6-31G method to perform extensive potential energy surface investigations. Throughout the paper our results refer to those obtained with the B3LYP/6-31G(d,p) method, except for the protonation studies, which are reported at the HF/6-31G level. For comparison, we present all the results for our key intermediate systems (**A**−**G**) computed with B3LYP/6-31G(d,p), B3LYP/6-31G, HF/631G(d,p) and HF/6-31G, in Table S1a in the Supporting Information. While differences between B3LYP and HF are not significant at the structural level (relevant distances are similar, as shown for **A**, in Table 1, within 0.001−0.15 Å), the relative energies exhibit some differences.

Computations were performed at NCI's Advanced Biomedical Computing Center (ABCC) and NCSA's SGI-Altix Teragrid.

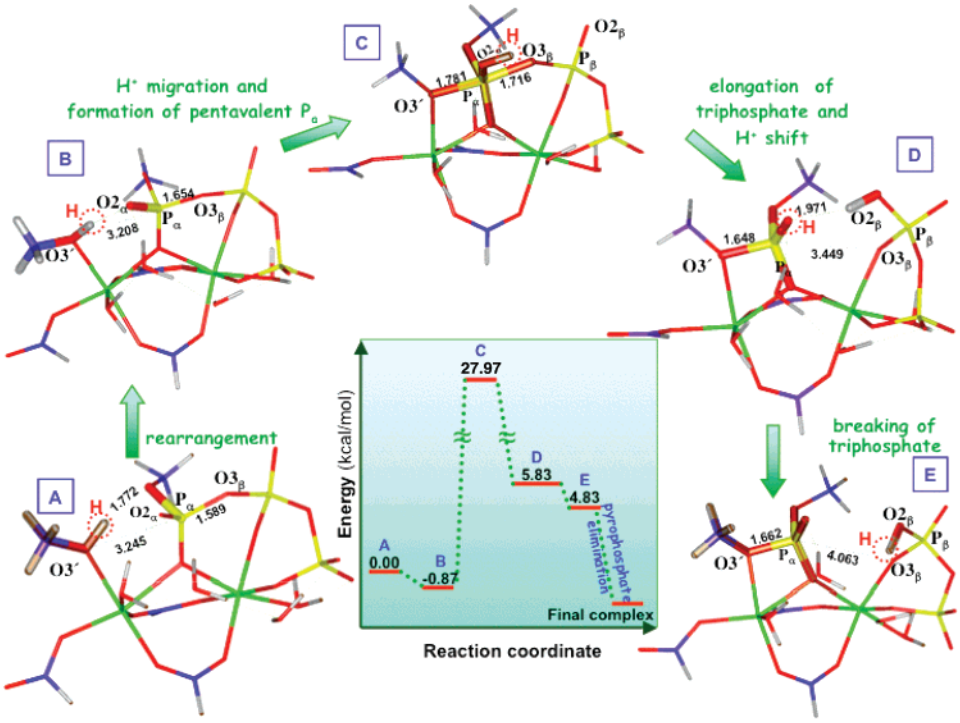

Figure 3. Reaction coordinate for the β-path, and the corresponding structures for each step. Thicker bonds represent the fragments that undergo major changes along the reaction coordinate. In all these structures Mg is green, P is yellow, O is red, C is blue, and H is gray. The shifting proton is highlighted by the red dotted circle. Energies (in kcal/mol) in bold are reported at the B3LYP/6-31G(d,p) level

For molecular images, we employ the graphics programs Insight II,[33a] Visual Molecular Dynamics (VMD),[33b] and ChemDraw 8.0.[33c]

Model Construction and Overview of Computations. Our model is based on the high-resolution (1.65 Å, *2fmp*) structure[11,12] derived from the refining of the ternary complex of polymerase β, primer terminus, and incoming nucleotide, shown in Figure 2, parts a and b. We substitute the crystal Na^+ by Mg^{2+} in the catalytic position and, because this structure does not have the essential OH groups on the primer and nucleotide, we insert them by replacing the corresponding hydrogen atoms on the ribose rings with OH units using Gaussview.[32]

To create a small but acceptable molecular system for a QM study, we eliminated residues not directly involved in the reaction, while retaining their electronic properties. Hence, all the aspartates are changed to formate ($HCOO^-$) ligands by modeling the rest of the side chain as a hydrogen.

As established in the refined X-ray structure of pol β, two coordinated water molecules are linked to each Mg^{2+} (catalytic and nucleotide-binding). Figure 1a shows the deoxynucleoside portions of the primer terminus and dCTP residues reduced to CH_3 groups; the models for these ligands become CH_3-OH and $[(CH_3-O-)P_3O_{10}]^{4-}$, respectively. This model is reasonable because our preliminary studies on larger systems showed that, when both the complete primer terminus and incoming nucleotide are present, the flexible ribose rings severely distort the system. These distortions can be prevented only by introducing special constraints to keep the incoming triphosphate and the primer rigid, which could result in a significant departure from the real mechanism. Our final QM model consists of 49 atoms and has an overall charge of -3.

All our model active sites have two unbound (crystallographic, free) water molecules (green in Figure 1a) linked only through hydrogen bonds to the rest of the complex, as they were located in the high-resolution structure. We term the water molecule coordinated to $Mg^{2+}{}_{cat}$ as $H_2O(1)$, and the water molecule directly hydrogen bonded to $H_2O(1)$ as $H_2O(2)$. In parallel, we study models without these free water molecules to assess their role and contribution to the reaction. We perform full optimizations of all intermediates with and without the crystallographic water molecules to accurately assess their energetic and structural effects on the reaction. We find that the noncovalently bound water molecules provide the framework for a strong hydrogen-bonding network, which compacts the complex as in the true enzymatic environment, and influence the relative energy of the systems by stabilizing them. However, there is no major structural difference between the pathways of the two sets of models, with or without the two crystallographic water molecules.

We present in the main text results for the models with two noncovalently bound water molecules and discuss those for the models without any crystallographic water molecules in the Supporting Information. We also describe an alternative pathway in which the proton is first transferred to the water coordinated to $Mg^{2+}{}_{cat}$, $H_2O(1)$, and later to $O2_\alpha$ via an unbound water, $H_2O(2)$, through a Grotthuss-type mechanism, an indirect variant for proton transfer, which lead to several key intermediates (**H** through **K**, in Figure S2 in the Supporting Information). All reported energies are relative to that of the optimized starting structure.

To capture the transitions from one intermediate to another (**A** through **E** in Figure 3), we performed several constrained optimizations, using the B3LYP/6-31G(d,p) method (data presented in the Supporting Information, Tables S5a, S5b, and S5c and Graphs G1a, G1b, and G1c). These studies helped estimate the energy barrier between **B** and **A** to 3.55 kcal/mol. Because we could not locate a transition state on the potential energy surface (PES) from **B** to **C**, we scanned the reverse reaction coordinate from **C** to **B** in two steps by employing first a series of constrained optimizations, to capture first the proton's rotation around the $O2_\alpha-P_\alpha$ bond, by changing the dihedral angle $O3_\beta-P_\alpha-O2_\alpha-H$ from $-90°$ to $90°$ while

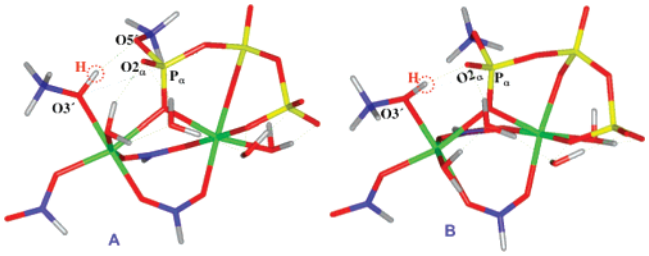

Figure 4. Initial, **A**, and rearranged, **B**, structures for the complex with two unbound waters. The green dashed lines represent hydrogen bonds.

keeping the proton on the same side with O5′ ("rotation above"), or from −90° to 90° while keeping the proton on the same side with $H_2O(2)$ ("rotation below"), followed by a proton shift from $O2_\alpha$ to O3′. Both pathways require about 15 kcal/mol (relative to **C**), indicating that the energy barrier needed to reach a transition state could be in this range. On the **D**−**C** (reverse β) and **F**−**C** (reverse γ) pathways, we shifted the proton from $O2_\beta$ to $O2_\alpha$, and $O2_\gamma$ to $O2_\alpha$, respectively, to determine which route was more favorable. We find that the β-pathway requires less energy, and thus is more likely.

We also examine the effect of placing one or two protons on the main intermediates to investigate the effect of protonation on the overall mechanism. In the Results section, we focus on the unprotonated species, but revisit the mechanism after one or two protons are included (Appendix). We discuss in the main text those cases in which the proton is added to complexes with two crystallographic waters, and in the Supporting Information the results obtained for the analogous complexes without crystallographic waters.

To probe the most favorable protonation positions, we placed the proton on each of the following seven sites, colored blue in Figure 1a. Namely, we survey all these possible locations around the catalytic magnesium site: (1) O^a of D256, (2−3) O^b of D256, at two different positions, one that leads to a dihedral angle O3′−Mg^{2+}_{cat}−O^b−C^{256} of 0° (Figure 1a) and another where this angle is 90° (and therefore the whole D256 unit is rotated, Figure 1b), (4) O^c of D190, (5) O^d of D192, (6) $O2_\gamma$ of P_γ (as proposed by Pedersen and collaborators), and (7) $O2_\beta$ of P_β.

The addition of a proton lowers the total charge of these molecular systems to −2, and if a second H^+ is inserted, the overall charge is further reduced to −1. Although a higher negative charge causes stronger electron−electron repulsions, we found that multiple protonations destabilize the system, as described below.

Results and Discussion

The overall reaction coordinate for our most favorable pathway, along with the energies associated with each intermediate, is presented in Figure 3. Our five key intermediates link the main steps in the reaction: rearrangement of the active site (from **A** to **B**), direct proton migration from O3′ to $O2_\alpha$ and formation of a pentavalent P_α center (**B** to **C**), elongation of one P_α−$O3_\beta$ bond (**C** to **D**), complete breaking of the P_α−$O3_\beta$ bond (**D** to **E**), and pyrophosphate elimination (**E** to a final, totally dissociated complex).

Recall that the starting point on our potential surface is the model molecule derived from the high-resolution pol β, with two unbound water molecules. Unconstrained minimizations lead to structure **A**, shown in Figures 3 and 4 (see Table 1 for key distances).

TABLE 1: Bond Distances for the Experimental and Computed Structure A, at the B3LYP(6-31G(d,p) and HF/6-31G Levels

bond	exptl structure, Å	computed structure **A**, Å B3LYP/6-31G(d,p) (HF/6-31G)
Mg^{2+}_{cat}−O3′	(2.706)[a]	2.218 (2.124)
Mg^{2+}_{cat}−$O1_\alpha$	2.497[a]	2.311 (2.357)
Mg^{2+}_{cat}−O (OH_2)	2.516[a]	2.148 (2.132)
Mg^{2+}_{cat}−O (D190)	2.284[a]	2.050 (2.039)
Mg^{2+}_{cat}−O (D192)	2.200[a]	2.073 (2.046)
Mg^{2+}_{cat}−O (D256)	2.372[a]	2.052 (2.030)
Mg^{2+}_{nuc}−$O1_\alpha$	2.082	2.176 (2.159)
Mg^{2+}_{nuc}−$O1_\beta$	2.037	2.137 (2.166)
Mg^{2+}_{nuc}−$O1_\gamma$	2.140	2.028 (2.013)
Mg^{2+}_{nuc}−O (OH_2)	2.149	2. 188 (2.187)
Mg^{2+}_{nuc}−O (D190)	2.091	2.090 (2.055)
Mg^{2+}_{nuc}−O (D192)	2.037	2.123 (2.087)
O3′−P_α	(4.112)[b]	3.245 (3.208)
H−O5′	(2.452)[b]	1.767 (1.802)
H−$O2_\alpha$	(4.125)[b]	2.966 (3.110)
Mg^{2+}_{cat}−Mg^{2+}_{nuc}	3.441[a]	3.712 (3.784)

[a] In the active site there is no O3′ or H, and a sodium ion resides in the position occupied by the catalytic magnesium ion. [b] Distances obtained after the missing OH groups were added with the Gaussview program

All distances from sodium (starred) in the experimental structure are, as expected, longer than those computed in which magnesium occupies the catalytic position. The bond lengths to Mg^{2+}_{nuc} are similar and the Mg^{2+}_{cat}−Mg^{2+}_{nuc} bond is longer in the calculated complex because our models have no constraints. We also illustrate in Table 1 the structural similarity of the computed structure **A**, when we employed two different sets of calculations: B3LYP/6-31G(d,p) and HF/6-31G.

Structure **A** has a hydrogen bond between H···O5′ but none to $O2_\alpha$ (red H is the proton on O3′(primer) that is released to initiate the reaction). This hydrogen has to shift to an adjacent atom to start the triphosphate dissociation reaction. The closest acceptor is the neighboring nucleotide oxygen, O5′, but this transfer is unproductive—it leads to the elimination of an alcohol before any changes in the triphosphate group can occur, forcing the reaction to terminate without DNA repair. Therefore, we searched for intermediates on the potential surface around **A** that have H pointing toward $O2_\alpha$, instead of O5′.

This produced a new minimum, **B** (Figure 4), in which the H (red) atom forms a hydrogen bond with $O2_\alpha$ (see Figure S1 in the Supporting Information for a superposition of **B** with **A**). **B** is 0.87 kcal/mol lower in energy than its isomer **A**, and has the O3′−$O2_\alpha$ bond at 3.097 Å, shorter by about 0.15 Å than in **A** (3.245 Å). Structure **B** is thus an excellent candidate to initiate the repair process. A survey of the potential energy surface via a series of constrained optimizations (Supporting Information, Table S5a and Graph G1a) revealed a 3.55 kcal/mol barrier from **A** to **B**. We report all energies for this system relative to **A**, at the B3LYP/6-31G(d,p) level.

Therefore, to start the reaction, no bond breaking or making is necessary, other than an initial step involving an energetically undemanding rearrangement of the complex, by a slight rotation of the catalytic Mg^{2+} octahedral environment with respect to the nucleotidic magnesium octahedron.

We also probed two intermediates resembling **A** and **B**, which have the O3′ proton pointing toward O(D256), as in the Pedersen et al. paper.[23a] While these new intermediates, **A**-like Pedersen and **B**-like Pedersen complexes, are comparable in energy to our intermediates **A** and **B** (the **A**-like Pedersen system is −0.15 kcal/mol lower in energy than **A**, and the **B**-like Pedersen

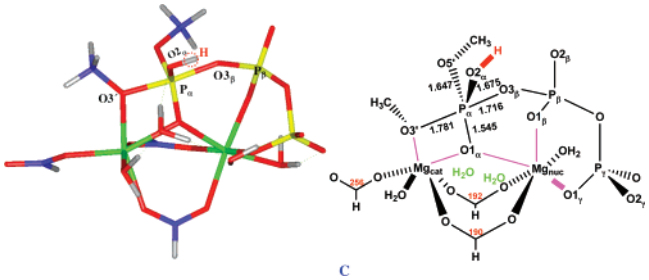

Figure 5. Intermediate, **C**, relevant bond distances, and notations for the main atoms (right). The green dashed lines show the main hydrogen network.

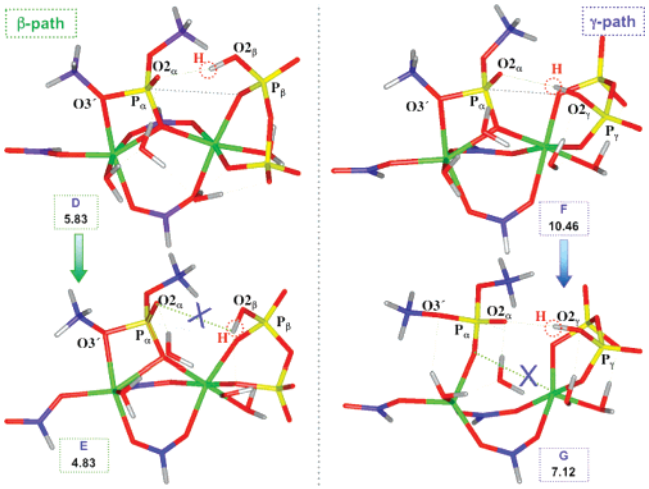

Figure 6. Intermediates on the β- (left) and γ- (right) pathways. **E** and **G** do not have hydrogen bonds between $O2_\alpha$ and $H(O_\beta)$, as represented by the blue **X**. Hydrogen bonds are the dashed green lines. Energies (in kcal/mol) are given at the B3LYP/6-31G(d,p) level.

complex is +1.95 kcal/mol higher than **B**, respectively), the O3′ to $O2_\alpha$ distances elongate significantly, from 3.245 Å in **A** to 3.672 Å in the **A**-like Pedersen molecule, and from 3.097 Å in **B** to 3.589 Å in its analogue, the **B**-like Pedersen complex. We thus conclude that our working intermediates, **A** and **B**, are more likely to participate in the repair process than their isomers, which have the O3′ proton H pointing toward D256.

After the direct proton shift from O3′ to $O2_\alpha$, O3′ becomes negatively charged and attacks P_α; this leads to the full dissociation of the triphosphate moiety. The resulting local minimum, **C**, is 27.97 kcal higher in energy relative to **A**, and has a trigonal bipyramidal P_α center. The axial bonds, O3′−P_α and P_α−$O3_\beta$, are 1.781 and 1.716 Å, respectively, longer than the equatorial contacts, P_α−$O2_\alpha$ = 1.675 Å, P_α−O5′ = 1.647 Å, or P_α−$O1_\alpha$ = 1.545 Å.

Potential energy surface scanning between **B** and **C** suggests, as described earlier, that there is a local maximum at 15 kcal/mol higher than **C** (Supporting Information, Table S5b and Graph G1b), for the above pathway, which is the most likely route.

Continuing along the reaction pathway, the proton is further transferred from $O2_\alpha$ to $O2_\beta$, a route that we call the β-pathway, we identify two intermediates: **D**, with a fully formed P_α−O3′ bond of 1.648 Å, and a nearly broken P_α−$O3_\beta$ bond, of 3.449 Å, held together by a strong hydrogen bond $O2_\alpha$···H−$O2_\beta$ of 1.971 Å, and **E** in which the pyrophosphate completely separates from P_α since no hydrogen bonds remain, with a P_α−$O3_\beta$ bond of 4.063 Å (Figure 6).

An alternative to transferring the proton from $O2_\alpha$ is to shift it to $O2_\gamma$ (γ-pathway). This pathway's two relevant intermediates are **F** and **G** (Figure 6). **F** has the pyrophosphate group separated from the original triphosphate unit, as the P_α−$O3_\beta$ bond is 3.225 Å, but contains a weaker $O2_\alpha$···H−$O2_\gamma$ hydrogen bond holding it together (2.118 Å), and a $Mg^{2+}{}_{nuc}$−$O1_\alpha$ bond almost equal to $Mg^{2+}{}_{cat}$−$O1_\alpha$ (2.142 Å, versus 2.172 Å); **G** does not have these two connections and evolves toward a finally dissociated product, as the P_α−$O3_\beta$ bond becomes 4.174 Å, $Mg^{2+}{}_{nuc}$−$O1_\alpha$ is 3.581 Å, and $Mg^{2+}{}_{cat}$−$O1_\alpha$ is 2.007 Å (Figure 6). Further studies of the reverse β- and γ-pathways by constrained minimizations revealed that there is a 3.44 kcal/mol energy barrier from **D** to **C** on the β-pathway, compared to 9.30 kcal/mol from **F** to **C** on the γ-pathway, shown in Table S5c and Graph G1c in the Supporting information.

Both pathways are plausible in an enzymatic environment, but the β-path is more likely because the final proton transfer is energetically less demanding (as both **D** and **E** are lower in energy than their counterparts on the γ-pathway, **F**, and **G**) and attainable because of the geometrical proximity between $O2_\alpha$···H−$O2_\beta$.

In the last step, the pyrophosphate is eliminated. A fully dissociated complex cannot be captured using our QM model, but we expect that QM/MM methods could locate it, as these calculations comprise the entire molecule.

Other Initial Proton-Transfer Steps. The first proton-transfer step, from O3′ to activate the primer, has been debated in the literature. It has been proposed that it occurs via one of the following three main routes: (1) directly to the adjacent $O2_\alpha$,[21,22] (2) to a neighboring aspartate unit,[20] or (3) to an H_2O or OH^- from the environment of the enzyme.[24,25]

The first case was discussed here and we find that it is geometrically and energetically the most probable.

The second instance (proton transfer to any adjacent aspartate), in the context of our computations (and models), is difficult to achieve geometrically, given that the hydrogen of O3′ points opposite to the D256 residue, or is orthogonal on D190 and D192, and thus a transition state on any of these pathways would entail a high-energy cost. QM/MM calculations in our group confirmed this.[23c] We summarize our findings in Table S2 in the Supporting Information.

Specifically, there are two possibilities for moving the proton (on each of these three intermediates) on D256: if the dihedral angle O3′−Mg_{cat}−O^{256}−H (Figure 1a) is 0°, then the D256−0 complex is formed; if it is 90°, then D256−90 is obtained. The former complex could be achieved from a simple proton shift, without the necessary mediation of a water molecule from the medium, whereas the latter could emerge only if a water molecule facilitated the proton migration. We found for D256−0 that the D256 bond to $Mg^{2+}{}_{cat}$ breaks, and D256−H^+ forms hydrogen bonds with O3′ or $H_2O(1)$. The O3′−P_α distance elongates significantly to 4.144 Å, beyond a reactive state. With the D256−90 structures, similar severe distortions occur, and none of the geometries are retained after optimizations. We also notice that complexes derived from **C** in which the proton H moves from $O2_\alpha$ to O(D256) are not stable, as the pentavalent P_α falls apart, so that a molecule with O3′ protonated and D256 departed from $Mg^{2+}{}_{cat}$, as described above, is formed. Aside from the migration of this H^+ back to the primer or to D256, a significant degradation of the active site occurs, as D256 leaves the catalytic site. Therefore, we argue that transferring the proton from O3′ to D256 (either orientation) is not a realistic relocation, within our model.

Proton transfer to D190 or D192 can occur by using only water molecules from the medium, since the primer and these two aspartates are too far from each other, making a direct move

energetically very costly. We find that placing the proton on either aspartate significantly deforms the structure of the resulting intermediates: the proton usually goes to D256, which leaves Mg^{2+}_{cat} to form hydrogen bonds with an oxygen of D190 or D192, respectively. Subsequently, the protonated D190, or D192, depart Mg^{2+}_{cat}, to form hydrogen bonds with D256. The results are summarized in the Supporting Information, Table S2.

Finally, the third possibility of proton transfer that we also examined involved the proton (H) shift from O3′ to the adjacent water molecule, $H_2O(1)$. We aimed to locate analogous intermediates to those found for $O2_\alpha(P_\alpha)$. Thus, we analyzed **A** (starting), **B** (rearranged species), and **C** (TS-like intermediate) analogous molecules, with two uncoordinated waters, which instead of having that particular proton on O3′, had it on H_2O-(1). This alternative route leads essentially to a pathway parallel to our main reaction coordinate, the direct transfer of the proton to $O2_\alpha$.

In this variant trajectory, the proton is first transferred from O3′, via the water coordinated to Mg^{2+}_{cat}, $H_2O(1)$, to an unbound water, $H_2O(2)$, and later to $O2_\alpha$, through a Grotthuss-type mechanism (an indirect proton-transfer mechanism).

We find four key intermediates (**H** through **K**, in Figure S2 in the Supporting Information). The first one, **H**, has the H on $H_2O(1)$, and is 9.70 kcal/mol higher in energy than **A**, and resembles **A**, structurally. As the proton migrates to $H_2O(2)$, and forms a hydrogen bond with $O2_\alpha$, a new intermediate emerges, **I**, 12.76 kcal/mol higher than **A**. Finally, as H is transferred to $O2_\alpha$ an intermediate similar to **C** arises, **K**, which has a trigonal bipyramidal P_α center, 33.75 kcal/mol above **A**, and about 6 kcal/mol higher than **C**. A fourth intermediate, **J**, closely resembles **I**, but it forms hydrogen bonds to $O2_\gamma$, instead of $O2_\alpha$, and is only 6.46 kcal/mol higher in energy than **A**. Thus, a proton transfer to $O2_\gamma$ is also a likely pathway.

These latter complexes suggest that alternative indirect proton transfers to $O2_\alpha$ or $O2_\gamma$ through a neighboring water molecule are plausible, in accord with Radhakrishnan and Schlick[23b] and Alberts et al.[23c]

Extracting the proton, by employing a hydroxyl group from the medium, is also possible, and was detailed by Warshel et al.,[25] but we have not analyzed it here.

Although a proton shift in the enzyme could occur to any of these adjacent oxygens, our computations indicate that the structures resulting from a direct transfer from O3′ to $O2_\alpha$ are structurally and energetically the most favorable.

We also examined seven protonation states highlighted in blue in Figure 1, and discussed these in detail in the Appendix as well as in the Supporting Information, Tables S3a and S3b (relative energies for the singly protonated complexes) and Tables S4a and S4b (for double protonations). We placed a proton on all the major intermediates (**A** through **G**) in those positions, and examined its effect on each structure.

Additionally, we analyzed several cases where two protons were added on both D256 and D190. All these structures are greatly perturbed, because the protonated D190 departs the Mg^{2+}_{nuc} site to form a bond only with Mg^{2+}_{cat}.

In general, when these intermediates are protonated, the structures are most often preserved, and resemble their unprotonated versions. Exceptions occur when the H^+ is added to D192, which once protonated leaves the system as $D192H^+$. Placing the proton on either $O2_\beta$ or $O2_\gamma$ leads to species considerably lower in energy than other protonated complexes (by at least 15 kcal/mol, at HF/6-31G level), particularly if H^+ is on $O2_\beta$.

It has been suggested that two protons could be added to this system to reduce the overall charge of the active site, and calculations with the PropKa program also prompted us to test this hypothesis. However, we found that double protonations greatly disturb the active site and thus we suggest that they are unlikely to occur. They significantly perturb the initial models, and we argue that if protons were present in an enzyme they would lead to detectable structural modifications, detectable by X-ray before initiating the reaction. Since none of the current data point to such substantial changes, we consider that these protonation variations (at the sites we studied) are less likely.

Conclusion

We have explored using QM methods several possible reaction pathways corresponding to the nucleotidyl transfer reaction, or the chemical step, in the cycle of polymerase β, by considering various initial proton-transfer steps as well as several protonation states of the active site aspartates and triphosphate. Our most favorable path involves as a first step a slight rearrangement in the geometry of the active site, by rotating the catalytic magnesium ion center. That first intermediate, **B**, lies at less than 1.0 kcal/mol below the starting point, as computed at the B3LYP/6-31G(d,p) level. Afterward, two major steps occur: (1) direct proton transfer from O3′(primer) to $O2_\alpha$-(P_α) leading to the formation of **C** that has a pentavalent P_α center and requires 27.97 kcal/mol and (2) dissociation of the triphosphate activated by a proton transfer to an oxygen of P_β, leading to **D**, followed by a full transfer of the nucleotide (**E**), which releases about 22 kcal/mol. Although this barrier is higher than the experimental value of 16 kcal/mol derived at room temperature from kinetic studies, the other QM/MM calculations also yield higher values. Clearly, the protein environment, not accounted for in our QM model, likely lowers this value. Direct proton shift from O3′ to $O2_\alpha$ emerges as the most favorable, when compared to other possibilities. The results indicate that chemistry is the rate-limiting overall step for correct nucleotide insertion in pol β, as previously determined.[23] An alternative route for the proton transfer, higher energetically by about 6 kcal/mol, occurs via two water molecules, one coordinated to Mg^{2+}_{cat} $H_2O(1)$, and one unbound, $H_2O(1)$, in a Grotthuss-type proton transfer, leading to four main intermediates that also produce a complex analogous to **C**. This pathway agrees with the findings of Radhakrishnan and Schlick[23b] and Alberts et al.[23c]

Our studies emphasize the multitude of pathways accessible in the complex enzymatic environment, given the possible variations in initial configurations, protonation states, and hydration levels. Protonation studies on the relevant intermediates suggest that adding a single H^+ to the system is possible, but the addition of a second proton significantly disturbs the active site. This implies that if the charge in the active site were reduced, the catalysis would still occur, as it does not interfere with the chemical step. We also found that the free water molecules are critical in maintaining the robustness of the active site, but their absence might not hamper the reaction. Finally, our results reinforce the notion that a rearrangement of the active site is essential in initiating the repair of the DNA in pol β. This involves the closely related "pre-chemistry" avenue concept,[19] which argues that stochastic adjustments of the active site are crucial to the incorporation of the incoming nucleotide, and that the differences in these pathways for various polymerases and systems (e.g., correct vs incorrect nucleotide incorporation) may help explain fidelity behavior in geometric and energetic terms. In addition, our higher energy than the experimental value of 16 kcal/mol underscores both the roles

of the tailored protein environment for the chemical reaction and the active-site arrangement that must occur to ready the system for the reaction. Studies on mismatched systems and other polymerases will help relate the conformational and chemical events to polymerase fidelity.

Acknowledgment. This work was supported by NSF Biophysics Grant MCB-0316771 and the donors of the Petroleum Research Fund (to T.S.), administered by the American Chemical Society. Research described in this article was also supported in part by Philip Morris USA Inc. and by Philip Morris International through an award to T.S. Computing resources provided by the NCSA and NCI supercomputing centers are greatly appreciated. We thank Dr. Ian Alberts, Ms. Meredith Foley, and Dr. Yanli Wang for reading our manuscript and their thorough comments. We thank Dr. Robert Rittenhouse for sharing his results with our group at NYU in December 2004 and discussing various aspects of DNA polymerase β chemical pathways.

Appendix: Discussion on Protonated Intermediates

Protonation Studies. Protonation is important in biological systems. A key problem in determining the exact number of protons in the active site is the complexity of the enzyme and our inability to pinpoint them experimentally or theoretically. For polymerase β a number of positions in the active site have been thought to be protonated, but the results are not consistent, as numerous factors affect the pK_a of each residue. The pK_a of an aspartate is about 3.9, and it could be unprotonated in enzyme (pK_a = 7.0). Various programs (PropKa, MCCE) protonate one or two residues (either the aspartates or the triphosphate), but they are not consistent in determining the exact location of the protons.

Single Protonations. We probed all our key intermediates (β- and γ-paths), as we discussed in the main text (nine intermediates with and nine without the two free waters), by surveying all possible locations for the proton around the catalytic magnesium site. For each set we tested seven protonation positions, shown in Figure 1, by fully relaxing the new structures (energies are given in Tables S3a and S3b in the Supporting Information). Here we discuss the results obtained for the intermediates with two unbound waters, but the outcome is similar for the complexes without noncovalently bound waters.

We find that if H^+ goes to O^a, then the O^b-C bond strengthens (to a partially double bond), and the O^b-Mg_{cat} bond weakens significantly, but if the proton is placed on O^b, then the O^a-C bond has a double bond character, and the O^b-Mg_{cat} bond weakens but less than in Figure 7 a. The same happens when either D190 or D192 get protonated, and O^c-Mg_{cat} becomes stronger than $O-Mg_{nuc}$, as illustrated in Figure 7c.

This proton reduces the charge on the model from -3 to -2. We find that structures are retained, except for the cases when the H^+ is added to D192, which leaves the active site.

The initial protonated molecules ($A-H^+$) closely resemble their unprotonated form, A. The protonated structures, $B-H^+$, have energies slightly lower than $A-H^+$ and also retain their unprotonated geometry, B. This implies that if protonation occurs, pol β's active site should resemble $B-H^+$ instead of A, with O3′H directed toward $O2_\alpha$, a finding not upheld experimentally. In $C-H^+$, the protonated D192 leaves the catalytic site, and thus the structure of the active site gets severely disturbed.

$D-H^+$ and $E-H^+$, intermediates on the β-path, have their final geometry similar to D, with the exception of the complexes

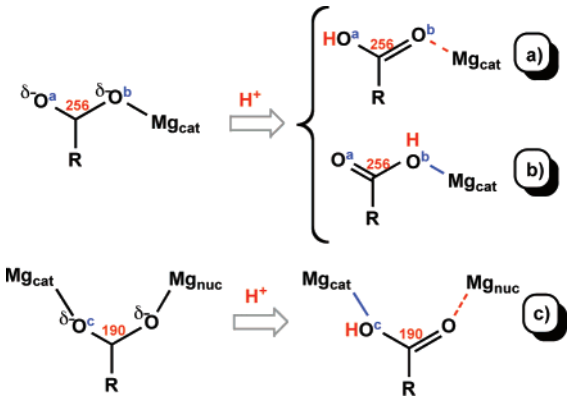

Figure 7. Coordination modes of the aspartates to the magnesium ions, and possible protonation sites (blue superscripts). Parts a and b present two bonding situations for D256, depending on the position of the proton, and part c shows the binding to D190, which is analogous to that in D192. Full blue lines denote a stronger bond, whereas the dotted red lines indicate weak interactions between oxygen and an adjacent magnesium center.

protonated at D190 or D192—these protonated aspartates leave the magnesium ions to form hydrogen bonds with D256. $F-H^+$ and $G-H^+$, intermediates on the γ-path, have the protonated D256, D190, and D192 leave the catalytic site, and sit higher in energy than $B-H^+$, making this route unlikely. The β-pathway is again energetically more favorable for the protonated complexes than the γ-path, and its structures are less disturbed.

Placing a proton on $O2_\beta(P_\beta)$ or $O2_\gamma(P_\gamma)$ leads to species significantly lower in energy than the other protonated complexes, the former being more favorable.

We conclude that although protonation decreases the charge of the final complexes, it also disturbs the active site, and that $O2_\beta(P_\beta)$ is the most favorable position. This is surprising, given that the pK_a computations focus on the pK_a values of the aspartates, and not on the acidity of the triphosphate unit.

Double Protonations. It has been proposed that two protons could be added to this system to reduce the overall charge of the active site, and calculations with the PropKa program also prompted us to test this hypothesis. The charge on our models is favorably reduced to -1. We placed the two protons on all our intermediates, on D256 and D190 (energies are given in Tables S4a and S4b in the Supporting Information).

In all the resulting molecules the protonated D190 either leaves the active site altogether or the Mg_{nuc} site and binds only to Mg_{cat}. Moreover, $B-2H^+$ intermediates are more stable than $A-2H^+$, as found in the case of single protonations, inconsistent with the experimental findings.

These significant structural perturbations should be detectable in the enzyme even before initiating the reaction, if they were to happen. Since none of the current data point to such substantial changes, we consider that a double protonation (at least at the sites we studied) is unrealistic.

Supporting Information Available: Figure S1 shows the overlap of **A** and **B**; Figure S2 shows the intermediates **H** and **K**; Table S1a provides relative energies for **A**−**G**, of the main intermediates at different levels of theory; Table S1b provides relative energies of the main intermediates at different levels of theory, with or without two unbound waters present in the active site; Table S2 contains relative energies (kcal/mol) for intermediates found in the alternative mechanisms discussed in the main text (when the proton migrates either to $O2_\alpha(P_\alpha)$, O(D256−0), O(D256−90), O(D190), or O(D192)), and a description of their structural features for the complexes with

two unbound waters, at the B3LYP-6-31G(d,p) level; Tables S3a and S3b present relative energies for protonated complexes, with and without noncovalently bound water molecules; Tables S4a and S4b present relative energies for the doubly protonated complexes, with and without noncovalently bound water molecules; Tables S5−7 show the energies found on the potential energy surfaces between **B** and **A**, **C** and **B**, **D**−C, and **F**−C, respectively; and Graphs G1−3 present the reaction coordinates for the **B** and **A**, **C** and **B**, **D**−C, and **F**−C transformations. This material is available free of charge via the Internet at http://pubs.acs.org.

References and Notes

(1) Vande Berg, B. J.; Beard, W. A.; Wilson, S. H. *J. Biol. Chem.* **2001**, *276*, 3408−3416.
(2) Beard, W. A.; Wilson, S. H. *Chem. Rev.* **2006**, *106*, 361−382.
(3) Mildvan, A. S. *Proteins*: *Struct. Funct. Genet.* **1997**, *29*, 401−416.
(4) Beese, L. S.; Steitz, T. A. *EMBO J.* **1991**, *10*, 25−33.
(5) Steitz, T. A. *J. Biol. Chem.* **1999**, *274*, 17395−17398.
(6) Steitz, T. A.; Smerdon, S. J.; Jager, J.; Joyce, C. M. *Science* **1994**, *266*, 2022−2025.
(7) Sawaya, M. R.; Pelletier, H.; Kumar, A.; Wilson, S. H.; Kraut, J. *Science* **1994**, *264*, 1930−1935.
(8) Steitz, T. A. *Nature* **1998**, *391*, 231−232.
(9) Beard, W. A.; Wilson, S. H. *Structure* **2003**, *11*, 489−496.
(10) Sawaya, M. R.; Prasad, R.; Wilson, S. H.; Kraut, J.; Pelletier, H. *Biochemistry* **1997**, *36*, 11205−11215.
(11) (a) Pelletier, H.; Sawaya, M. R.; Wolfle, W.; Wilson, S. H.; Kraut, J. *Biochemistry* **1996**, *35*, 12742−12761. (b) Pelletier, H.; Sawaya, M. R.; Wolfle, W.; Wilson, S. H.; Kraut, J. *Biochemistry* **1996**, *35*, 12762−12777. (c) Pelletier, H.; Sawaya, M. R.; Kumar, A.; Wilson, S. H.; Kraut, J. *Science* **1994**, *264*, 1891−1903. (d) Eckert, K. A.; Opresko, P. L. *Mutat. Res.* **1999**, *424*, 221−236.
(12) Batra, V. K.; Beard, W. A.; Shock, D. D.; Krahn, J. M.; Pedersen, L. C.; Wilson, S. H. *Structure* **2006**, *14*, 757−766.
(13) Batra, V. K.; Beard, W. A.; Shock, D. D.; Pedersen, L. C.; Wilson, S. H. *Structure* **2005**, *13*, 1225−1233.
(14) Filee, J.; Forterre, P.; Sen-Lin, T.; Laurent, J. *J. Mol. Evol.* **2002**, *54*, 763−773.
(15) Lahiri, S. D.; Zhang, G.; Dunaway-Mariano, D.; Allen, K. N. *Science* **2003**, *299*, 2067−2071.
(16) Yang, L.; Arora, K.; Beard, W. A.; Wilson, S. H.; Schlick, T. *J. Am. Chem. Soc.* **2004**, *126*, 8441−8453.
(17) Arora, K.; Beard, W. A.; Wilson, S. H.; Schlick, T. *Biochemistry* **2005**, *44*, 13328−13341.
(18) Arora, K.; Schlick, T. *J. Phys. Chem. B* **2005**, *109*, 5358−5367.
(19) (a) Radhakrishnan, R.; Schlick, T. *PNAS* **2004**, *101*, 5970−5975. (b) Arora, K; Schlick, T. *Biophys. J.* **2004**, *87*, 1−12.
(20) (a) Radhakrishnan, R.; Schlick, T. *J. Am. Chem. Soc.* **2005**, *127*, 13245−13252. (b) Radhakrishnan, R.; Arora, K.; Wang, Y.; Beard, W. A.; Wilson, S. H.; Schlick, T. *Biochemistry* **2006**, *45*, 15142−15156.
(21) Abashkin, Y. G.; Erickson, J. W.; Burt, S. K. *J. Phys. Chem. B* **2001**, *105*, 287−292.
(22) Rittenhouse, R. C.; Apostoluk, W. K.; Miller, J. H.; Straatsma, T. P. *Proteins* **2003**, *53*, 667−682.
(23) (a) Lin, P.; Pedersen, L. C.; Batra, V. K.; Beard, W. A.; Wilson, S. H.; Pedersen L. G. *PNAS* **2006**, *103*, 13294−13299. (b) Radhakrishnan, R.; Schlick, T. *BBRC* **2006**, *350*, 521−529. (c) Alberts, I.; Wang, Y.; Schlick, T. *J. Am. Chem. Soc.* Submitted for publication.
(24) Florian, J.; Goodman, M. F.; Warshel, A. *PNAS* **2005**, *102*, 6819−6824.
(25) Florian, J.; Goodman, M. F.; Warshel, A. *J. Am. Chem. Soc.* **2003**, *125*, 8163−8177.
(26) Xiang, Y.; Oelschlaeger, P.; Florian, J.; Goodman, M. F.; Warshel, A. *Biochemistry* **2006**, *45*, 7036−7048.
(27) Dittrich, M.; Hayashi, S.; Schulten, K. *Biophys. J.* **2003**, *8*, 2253−2266.
(28) (a) Hartree, D. R. *Proc. Cambridge Philos. Soc.* **1928**, *24*, 111−132. (b) Hartree, D. R. *The Calculation of Atomic Structures*; Wiley-Interscience: New York, 1957. (c) Fock, V. A. *Z. Phys.* **1930**, *61*, 126−135. (d) Fock, V. A. *Z. Phys.* **1930**, *62*, 795−801.
(29) (a) Becke, A. D. *J. Chem. Phys.* **1993**, *98*, 5648−5652. (b) Becke, A. D. *J. Chem. Phys.* **1993**, *98*, 1372−1377. (c) Lee, C.; Yang, W.; Parr, R. G. *Phys. Rev. B* **1988**, *37*, 785−789. (d) Stephens, P. J.; Devlin, F. J.; Chabalowski, C. F.; Frisch, M. J. *J. Phys. Chem.* **1994**, *98*, 11623−11627.
(30) (a) Møller, C.; Plesset, M. S. *Phys. Rev.* **1934**, *46*, 618−622. (b) Head-Gordon, M.; Pople, J. A.; Frisch, M. J. *Chem. Phys. Lett.* **1988**, *153*, 503−506. (c) Frisch, M. J.; Head-Gordon, M.; Pople, J. A. *Chem. Phys. Lett.* **1990**, *166*, 275−280. (d) Frisch, M. J.; Head-Gordon, M.; Pople, J. A. *Chem. Phys. Lett.* **1990**, *166*, 281−289. (e) Head-Gordon, M.; Head-Gordon, T. *Chem. Phys. Lett.* **1994**, *220*, 122−128. (f) Saebo, S.; Almlof, J. *Chem. Phys. Lett.* **1989**, *154*, 83−89.
(31) (a) Ditchfield, R.; Hehre, W. J.; Pople, J. A. *J. Chem. Phys.* **1971**, *54*, 724−728. (b) Hehre, W. J.; Ditchfield, R.; Pople, J. A. *J. Chem. Phys.* **1972**, *56*, 2257−2261. (c) Hariharan P. C.; Pople, J. A. *Mol. Phys.* **1974**, *27*, 209−214. (d) Gordon, M. S. *Chem. Phys. Lett.* **1980**, *76*, 163−168. (e) Hariharan, P. C.; Pople, J. A. *Theor. Chim. Acta* **1973**, *28*, 213−222. (f) Blaudeau, J.-P.; McGrath, M. P.; Curtiss, L. A.; Radom, L. *J. Chem. Phys.* **1997**, *107*, 5016−5021. (g) Francl, M. M.; Pietro, W. J.; Hehre, W. J.; Binkley, J. S.; Gordon, M. S.; DeFrees, D. J.; Pople, J. A. *J. Chem. Phys.* **1982**, *77*, 3654−3665. (h) Binning, R. C., Jr.; Curtiss, L. A. *J. Comput. Chem.* **1999**, *11*, 1206−1216. (i) Rassolov, V. A.; Pople, J. A.; Ratner, M. A.; Windus, T. L. *J. Chem. Phys.* **1998**, *109*, 1223−1229. (j) Rassolov, V. A.; Ratner, M. A.; Pople, J. A.; Redfern, P. C.; Curtiss, L. A. *J. Comput. Chem.* **2001**, *22*, 976−984.
(32) Dennington, R., II; Keith, T.; Millam, J.; Eppinnett, K.; Hovell, W. L.; Gilliland, R. *GaussView*, Version 3.09; Semichem, Inc.: Shawnee Mission, KS, 2003.
(33) (a) *Insight II*, version 2005; Accelrys, Cambridge, U.K.; http://www.accelrys.com/products/insight/index.html. (b) Humphrey, W.; Dalke, A.; Schulten, K. VMD-Visual Molecular Dynamics, version 1.8.3. *J. Mol. Graphics* **1996**, *14*, 33−38. (c) *ChemDraw Ultra*, Version 8.0; CambridgeSoft.com: Cambridge, MA.
(34) Frisch, M. J.; Trucks, G. W.; Schlegel, H. B.; Scuseria, G. E. M.; Robb, A.; Cheeseman, J. R.; Zakrzewski, V. G.; Montgomery, J. A.; Stratmann, R. E.; Burant, J. C.; Dapprich, S.; Millam, J. M.; Daniels, A. D.; Kudin, K. N.; Strain, M. C.; Farkas, O.; Tomasi, J.; Barone, V.; Cossi, M.; Cammi, R.; Mennucci, B.; Pomelli, C.; Adamo, C.; Clifford, S.; Ochterski, J.; Petersson, G. A.; Ayala, P. Y.; Cui, Q.; Morokuma, K.; Malick, D. K.; Rabuck, A. D.; Raghavachari, K.; Foresman, J. B.; Cioslowski, J.; Ortiz, J. V.; Stefanov, B. B.; Liu, G.; Liashenko, A.; Piskorz, P.; Komaromi, I.; Gomperts, R.; Martin, R. L.; Fox, D. J.; Keith, T.; Al-Laham, M. A.; Peng, C. Y.; Nanayakkara, A.; Gonzalez, C.; Challacombe, M.; Gill, P. M. W.; Johnson, B. G.; Chen, W.; Wong, M. W.; Andres, J. L.; Head-Gordon, M.; Replogle, E. S.; Pople, J. A. *Gaussian 98*, Gaussian, Inc.: Pittsburgh, PA, 1998.
(35) propka.chem.uiowa.edu/.